2007

In Vivo Imaging of Transport and Biocompatibility of Single Silver Nanoparticles in Early Development of Zebrafish Embryos

Kerry J. Lee
Old Dominion University, kleex008@gsa.odu.edu

Prakash D. Nallathamby
Old Dominion University, pnall002@gsa.odu.edu

Lauren M. Browning
Old Dominion University, lbrownin@odu.edu

Christopher J. Osgood
Old Dominion University, cosgood@odu.edu

Xiao-Hong Nancy Xu
Old Dominion University, xhxu@odu.edu

Original Publication Citation

Lee, K. J., Nallathamby, P. D., Browning, L. M., Osgood, C. J., & Nancy Xu, X. H. (2007). In vivo imaging of transport and biocompatibility of single silver nanoparticles in early development of zebrafish embryos. *ACS Nano, 1*(2), 133-143. doi:10.1021/nn700048y

Published in final edited form as:
ACS Nano. 2007 September 28; 1(2): 133–143. doi:10.1021/nn700048y.

In Vivo Imaging of Transport and Biocompatibility of Single Silver Nanoparticles in Early Development of Zebrafish Embryos

Kerry J. Lee[1,¶], **Prakash D. Nallathamby**[1,¶], **Lauren M. Browning**[1], **Christopher J. Osgood**[2], and **Xiao-Hong Nancy Xu**[1,*]

1*Department of Chemistry and Biochemistry, Old Dominion University, Norfolk, VA 23529*

2*Department of Biological Sciences, Old Dominion University, Norfolk, VA 23529*

Abstract

Real-time study of transport and biocompatibility of nanomaterials in early embryonic development at single-nanoparticle resolution can offer new knowledge about their delivery and effects *in vivo*, and provide new insights into molecular transport mechanism of developing embryos. In this study, we directly characterized transport of single silver (Ag) nanoparticles into an *in vivo* model system (zebrafish embryos) and investigated their effects on early embryonic development at single-nanoparticle resolution in real-time. We designed highly purified and stable (not aggregated and non-photodecomposition) nanoparticles and developed single-nanoparticle optics and *in vivo* assays to enable the study. We found that single Ag nanoparticles (5–46 nm) transport in and out of embryos through chorion pore canals (CPCs), and exhibit Brownian diffusion (not active transport) with ~26 times lower diffusion coefficient (3×10^{-9} cm^2/s) inside the chorionic space than in egg water (7.7×10^{-8} cm^2/s). In contrast, nanoparticles were trapped inside CPCs and inner mass of embryos, showing restricted diffusion. Individual Ag nanoparticles were observed inside embryos at each developmental stage, and in normally developed, deformed, and dead zebrafish, showing that biocompatibility and toxicity of Ag nanoparticles and types of abnormalities of zebrafish highly depend on the dose of Ag nanoparticles with a critical concentration of 0.19 nM. Rates of passive diffusion and accumulation of nanoparticles in embryos are likely responsible for the dose-dependent abnormalities. Unlike other chemicals, single nanoparticles can be directly imaged inside developing embryos at nanometer (nm) spatial resolution, offering new opportunities to unravel the related pathways that lead to the abnormalities.

Keywords

Biocompatibility; diffusion; embryos; in vivo imaging; silver nanoparticle; single nanoparticle optics; toxicity; transport; zebrafish

Introduction

Nanomaterials possess unique physical and surface properties, which have inspired plans for a wide spectrum of applications, such as target-specific vehicles for *in vivo* sensing, diagnosis, and therapy (e.g., nanomedicine, drug delivery).[1–5] These unique properties may also incite toxicity, damaging *in vivo* systems of interest and posing risks to human health and the environment.[6] Thus, we select an effective *in vivo* model system (zebrafish embryos) and one type of nanomaterials (Ag nanoparticles) and focus on probing the transport mechanism and

*To whom correspondence should be addressed: Email: xhxu@odu.edu; www.odu.edu/sci/xu/xu.htm; Tel/fax: (757) 683-5698.
¶These authors contributed equally to this work.

dose-dependent biocompatibility of the nanomaterials *in vivo*, targeting the initial entry step of nanomaterials into embryos, and aiming to demonstrate its potential applications and address its potential adverse effects. Real-time study of transport and biocompatibility of single nanoparticles in early development of embryos will provide new insights into molecular transport mechanism and structure of developing embryos at nanometer (nm) spatial resolution *in vivo*, as well as assessing the biocompatibility of single nanoparticle probes *in vivo*.

Currently, fluorescent probes, such as fluorescent dyes and proteins, are commonly used probes for *in vivo* imaging. Unfortunately, fluorescence probes suffer photodecomposition, offering limited lifetime for probing dynamic events of interest. Recently, nanoparticle probes such as semiconductor quantum dots (QDs) and noble metal nanoparticles are becoming popular and powerful probes for living cellular and *in vivo* imaging.[7–12] QDs have unique optical properties in comparison with fluorescence dyes and proteins, such as tunable narrow emission spectrum, broad excitation spectrum, high photostability, and long fluorescence lifetime.[8, 9, 13] Nevertheless, QDs still suffer a certain degree of photodecomposition, and it remains a challenge to prevent intracellular QDs from aggregation.

Noble metal nanoparticles (Ag, Au and their alloys) have unique optical properties, such as surface plasmon resonance (SPR), showing the dependence of optical properties on their size, shape, surrounding environment, and dielectric constant of the embedding medium.[14–17] Recent research has demonstrated the feasibility of using intrinsic optical properties of the nanoparticles for imaging single living cells in real-time with sub-100 nm spatial resolution and millisecond time resolution.[10–12] Among noble metal nanoparticles, Ag nanoparticles offer the highest quantum yield (QY) of Rayleigh scattering. For example, the QY of Rayleigh scattering of 2 nm Ag nanoparticles is about 10^4 times higher than that of a single fluorescent dye molecule (e.g., Rhodamine 6G). The scattering intensity of noble metal nanoparticles is proportional to the volume of nanoparticles.[14–17] Thus, Ag nanoparticles are extremely bright and can be directly observed using dark-field single nanoparticle optical microscopy and spectroscopy (SNOMS). Unlike fluorescent probes and QDs, these noble metal nanoparticles do not suffer photodecomposition and can be used as a probe to continuously monitor dynamic events for an extended period of time. Furthermore, the localized surface plasmon resonance (LSPR) spectra (color) of nanoparticles show size-dependence.[14–16] Thus, one can use the color (LSPR spectra) index of these multicolor nanoparticles as a nanometer-size index (CASI) to directly measure membrane transports of nanoparticles and size the change of membrane pores at the nanometer scale in real-time. [10–12]

Nevertheless, like other nanoparticle probes (e.g., QDs), the biocompatibility of Ag nanoparticles awaits further and systematic study.[6, 12] Thus, it is important to develop *in vivo* model systems to effectively screen biocompatibility of nanoparticle probes in real-time while exploring the potential of nanoparticles for *in vivo* imaging.

Zebrafish (*Danio rerio*) have unique advantageous features over other vertebrate model systems (e.g., mouse, rat, human).[18–22] For example, its early embryonic development is completed rapidly within 120 h with well-characterized developmental stages. The embryos are transparent and develop outside of their mothers, permitting direct visual detection of pathological embryonic death, mal-development phenotypes, and study of real-time transport and effects of nanoparticles *in vivo*. Therefore, zebrafish embryos offer a unique opportunity to investigate the effects of nanoparticles upon intact cellular systems that communicate with each other to orchestrate the events of early embryonic development. Genetic screens of zebrafish phenotypes indicate similarities to human diseases, and protein sequences of drug-binding sites in zebrafish and human show a high degree of identities.[18, 22] Thus, zebrafish have served as a vital model system for screening drug targets for curing human diseases. Large numbers of embryos can be generated rapidly at low cost, which can serve as an ideal *in*

vivo assay for screening biocompatibility, pharmacological efficacy, and toxicity of nanoparticle probes. Fish are renowned for their ability to bioconcentrate trace contaminants in the environment. Human consumption of fish suggests a direct impact to human health by potential releases of nanomaterials into the environment.

Although the zebrafish has been a popular model for screening chemical toxicity[19] and drugs[22], it has not yet been reported for screening the biocompatibity, therapeutic effects and toxicity of nanoparticles. Furthermore, in all reported nanotoxicity studies, conventional toxicological assays were primarily used, which cannot characterize dose of nanoparticles *in vivo* and in real time. Typically, nanoparticles were injected into *in vivo* systems[6, 23], which is highly invasive. Many of these studies used unpurified nanoparticles or functionalized nanoparticles and did not consider effects of residual chemicals produced during nanoparticle synthesis persisting in nanoparticle solutions, leading to inconclusive results.[6]

Currently, biocompatibility of nanoparticles used as labeling agents for imaging of cells and organisms quite often is not well-characterized. The primary challenges of using nanoparticle probes for *in vivo* imaging and probing the effects of nanoparticles on living cells and organisms are (i) to maintain the stability (prevent aggregation and photodecomposition) of nanoparticles in physiological medium and *in vivo*, (ii) to develop real-time imaging tools for tracking the diffusion and location of individual nanoparticles *in vivo*, and (iii) to invent powerful means to characterize individual nanoparticles *in vivo* and in real time. In this study, we have accomplished all of these objectives, achieving a major advance in the study of single nanoparticles *in vivo*.

Results and Discussion

Synthesis and characterization of Ag nanoparticles

We synthesized spherical Ag nanoparticles with average diameter of (11.6 ± 3.5) nm by reducing $AgClO_4$ with reducing agents (sodium citrate and sodium borohydride) using well-tuned synthesis conditions as described in Methods. We then carefully washed nanoparticles to remove trace chemicals from their synthesis using centrifugation, generating highly purified nanoparticles. We characterized the stability, size and optical properties of these purified Ag nanoparticles incubated in egg water (1.2 mM NaCl) for 120 hr using UV-vis absorption spectroscopy, SNOMS, dynamic light scattering (DLS), and high-resolution transmission electron microscopy (HR-TEM) (Fig. 1).

The absorption spectra of freshly prepared and washed nanoparticles before and after incubating with egg water for 120 hr (Figs. 1A: a & b) show an absorbance of 0.736 at a peak wavelength of 396–400 nm, indicating that Ag nanoparticles are very stable (not aggregated) in egg water (1.2 mM NaCl). We determined the effect of salt concentration (the positive control experiment) by increasing NaCl concentration and found that nanoparticles are stable in the presence of NaCl up to 10 mM, but begin to aggregate in 100 mM NaCl, showing a red shift of peak absorbance wavelength (~2–3 nm) and a decrease in absorbance. The size of nanoparticles measured by DLS increased from (10.1 ± 2.0) nm to (24.4 ± 2.7) nm in the presence of 100 mM NaCl. The presence of sufficiently high concentration of NaCl (100 mM) appears to reduce the thickness of electric double-layer on the surface of nanoparticles and decrease the zeta potential below its critical point, leading to aggregation of nanoparticles.

We characterized the size of Ag nanoparticles using HR-TEM and DLS before and after incubating with egg water for 120 hr, showing that the size of nanoparticles remained unchanged with an average diameter of 11.6 ± 3.5 nm.

Furthermore, we characterized the optical properties of individual nanoparticles using SNOMS (Figs. 1: C–F). A representative optical image of single nanoparticles in Fig. 1C illustrates that the majority of nanoparticles are blue with some being green and few are red. The representative LSPR spectra of single blue, green and red nanoparticles show a peak wavelength at 488, 532 and 607 nm (Fig. 1D), respectively. The correlation of the color distribution of individual nanoparticles with their size measured by HR-TEM, shows the majority (74%) of single nanoparticles with diameters of 5–15 nm are blue, 23% of single nanoparticles with diameters of 16–30 nm are green, and a very small fraction (1%) of nanoparticles (31–46 nm) are red (Fig. 1E). Thus, the color-index of single nanoparticles can be used as a size-index to directly distinguish and determine the size of nanoparticles (5–46 nm) using SNOMS, even though the size of nanoparticles cannot be directly measured due to the optical diffraction limit. We also found that the distribution of color and size of nanoparticles remained unchanged as nanoparticles were incubated in egg water for 120 hr, suggesting that nanoparticles are stable (not aggregated) in egg water at single-nanoparticle resolution.

To determine the photostability of Ag nanoparticles, we acquired sequence images of single Ag nanoparticles while these nanoparticles were constantly radiated under a dark-field microscope illuminator (100 W halogen) for 12 hr. The illumination power at the sample stage (focal plane of dark field) was 0.070 ± 0.001 Watt. Representative plots of scattering intensity of single nanoparticles and background (in the absence of nanoparticles) versus illumination time in Fig. 1F indicate that the scattering intensity of individual single nanoparticles remains unchanged over 12 hr, showing that single Ag nanoparticles resist photodecomposition and blinking. Note that the small fluctuations of intensity of single nanoparticles (Fig. 1F: i) are similar to those observed from the background (Fig. 1F: ii), suggesting that the intensity fluctuations are attributable to the illuminator and the noise level of the CCD camera.

Probing diffusion and transport of single nanoparticles in cleavage stage embryos

Representative developmental stages of the zebrafish embryos in 120 hour-post-fertilization (hpf) in Fig. 2 show the cleavage stage (8–64 cell stages), segmentation stage, hatching stage, and pharyngula stage embryos, and a fully developed zebrafish in the absence of nanoparticles. At the cleavage-stage (8–64 cell stage; 0.75–2.25 hpf) (Fig. 2A–B), embryos undergo dramatic changes (e.g., rapid cellular division and distinct fate establishment) to lay down the foundation for developing the different parts of organs and a variety of interesting but not yet well-understood biochemical and biophysical events (e.g., cell migration signaling and embryonic pattern formation) occur. This stage is crucial in development as the foundation and organization of the embryos are being assembled.[24, 25] Thus, it is important to understand the diffusion and transport mechanisms among the various parts of embryos at this particular stage. The cleavage stage embryos may also be most sensitive to foreign substances[26], offering an ultrasensitive *in-vivo* model system to study the biocompatibility and subtle effects of nanoparticles on the embryonic development.

To study diffusion and transport of single nanoparticles into cleavage stage embryos, we incubated Ag nanoparticles with the embryos and directly observed and characterized their transport, showing that Ag nanoparticles (blue, green and red) transport into the chorionic space (cs) via chorion pore canals (CPCs) and enter into the inner mass of embryo (ime) (Fig. 3 and Movie 1–Movie 2). We used our optical imaging system to directly measure the diameters of chorion pore canals, showing them to be approximately 0.5–0.7 μm in diameter with distances between the centers of two nearby chorion pore canals are at ~1.5–2.5 μm, which agrees well with those reported using TEM.[27] To our knowledge, this study demonstrates for the first time direct observation of chorionic pore canals of single living embryos using optical microscopy. We show that the sizes of chorion pore canals are larger than the size of nanoparticles,

permitting the passive diffusion of individual nanoparticles into the chorionic space of embryos.

To determine the transport mechanism of Ag nanoparticles, we utilized the concept of 2D mean-square-displacement (MSD) and diffusion models (e.g., directed, simple and stationary Brownian diffusion)[28, 29] to investigate each diffusion trajectory of single nanoparticles in egg water, entry into embryos, and inside embryos. To follow the diffusion of single nanoparticles inside various parts of embryos in real-time, we used real-time square-displacement (RTSD) (diffusion distance at a given time interval), instead of average (mean) of square-displacement over time, because the diffusion coefficient could vary as single nanoparticles diffuse in embryos. This approach allowed us to probe the diffusion of single nanoparticles and viscosity of the different parts of embryonic fluids (e.g., chorionic space, inner mass of embryo) in real-time. The diffusion coefficient (D) of single nanoparticles in simple Brownian motion is calculated by dividing the slope of a linear plot of real-time square-displacement versus time by 4 (Note: RTSD = $4D\Delta t$) (Fig. 4B).

Representative diffusion trajectories of single Ag nanoparticles trapped inside chorion pore canals, in chorionic space and near the inner mass of embryo, and analysis of these diffusion trajectories using the real-time square-displacement method are shown in Fig. 4. The results illustrate that single Ag nanoparticles inside the chorionic space (either near the chorion layers or inner mass of the embryo) exhibit simple Brownian diffusion (not active transport) with ~26 times slower diffusion rate (3×10^{-9} cm^2/s) than those in egg water (7.7×10^{-8} cm^2/s), showing that single Ag nanoparticles diffuse into the chorionic space via passive diffusion and that the viscosity of chorionic space is about 26 times higher than that of egg water.

As nanoparticles make several attempts to enter the chorion layers and inner mass of the embryo, their diffusion patterns are restricted (Fig. 4B: a–i, steps in a-ii and a-iii), suggesting that the nanoparticles dock into the chorion pore canals, which halts their normal diffusion. By tracking the entry of individual nanoparticles into chorion pore canals, we measured the period of time that individual nanoparticles stay in the pores, which ranges from 0.1 to 15 s.

We characterized the diffusion coefficient of blue, green and red nanoparticles in egg water (Fig. 4B: b) to determine the possible variation of diffusion coefficients due to the different sizes (radii) of single nanoparticles, showing simple Brownian diffusion with D of 8.4 $\times10^{-8}$, 6.0 $\times10^{-8}$ and 5.5 $\times10^{-8}$ cm^2/s, respectively. The diffusion coefficients are inversely proportional to their radius, as described by the Stoke-Einstein equation, $D = kT/(6\pi\eta a)$, showing that the diffusion coefficient (D) depends on the viscosity of medium (η) and the radius (a) of solute (nanoparticle).[30, 31] The diffusion coefficients of the given color (radius) of nanoparticles in embryos were studied and compared with those in egg water, showing that the various diffusion coefficients observed in three different parts of embryos (Fig. 4B: a) were indeed attributable to the viscosity gradient inside embryos, but not the different radii of individual nanoparticles.

Characterization of transport and embedded nanoparticles

Images of single nanoparticles transporting into the chorionic space were recorded using dark-field SNOMS equipped with a color camera, instead of CCD, showing that nanoparticles of multiple colors transport into the chorionic space (Fig. 5A). Note that single Ag nanoparticles exhibit colors (LSPR), which depends on its size, shape and surrounding environments.[14–17] This feature allowed us to distinguish single Ag nanoparticles from any possible tissue debris or vesicle-like particles in embryos, which do not exhibit surface plasmon and hence appear white under dark-field microscope (Fig. 3 & Fig. 4). We found that the majority of nanoparticles transported into the chorionic space and some of them overlapped with chorion pore canals (Fig. 5A: a). The representative LSPR spectra (colors) of individual nanoparticles

inside chorionic space (Fig. 5A: b) show similar peak wavelengths as those observed in egg water in Fig. 1D. The results indicate that the majority of nanoparticles remained non-aggregated inside embryos. Otherwise, we would have observed a significant red shift of LSPR spectra of individual nanoparticles.

Although the majority of single nanoparticles can freely diffuse into embryos and remain non-aggregated, some single nanoparticles stay in chorion pore canals for an extended period of time. These trapped nanoparticles serve as nucleation sites and aggregate with incoming nanoparticles to form larger particles (dark-red nanoparticles) (Fig. 5B), clogging chorion pore canals and affecting the embryo's transport. Note that, embryos at this developmental stage are free of pigmentation.

As the cleavage (8-cell) stage embryos chronically treated with lower concentrations of Ag nanoparticles (< 0.08 nM) completed their embryonic development at 120 hpf, we characterized Ag nanoparticles embedded in fully developed zebrafish using SNOMS and found that these Ag nanoparticles embedded in multiple organs (retina, brain, heart, gill arches, and tail) of normally developed zebrafish (Fig. 6), demonstrating that Ag nanoparticles are biocompatible to embryos at lower concentrations (< 0.08 nM). The LSPR spectra of these embedded nanoparticles are similar to those observed in Fig. 5A:b. We also performed blank control experiments by imaging 120-hpf zebrafish that developed in the absence of nanoparticles and did not observe the signature LSPR spectra (color) of Ag nanoparticles in these fully developed zebrafish.

Dose-dependent biocompatibility and toxicity

To determine the effect of dose of Ag nanoparticles on the embryonic development, we treated the cleavage stage (8-cell stage) embryos chronically with various concentrations of Ag nanoparticles (0 – 0.71 nM) and carefully monitored and characterized their vital developmental stages (24, 48, 72, 96, and 120 hpf). The results in Fig. 7 show that biocompatibility of Ag nanoparticles and the types of abnormalities in treated zebrafish are highly dependent on the dose of Ag nanoparticles. In the presence of lower concentrations (< 0.08 nM) of nanoparticles, a higher percentage of normally developed zebrafish is observed than that of dead and deformed zebrafish. Note that both normal and deformed zebrafish developed from the cleavage (8-cell) stage embryos that had been simultaneously incubated with the same nanoparticle solution. Thus, the results suggest that some embryos might be more tolerant to the nanoparticles than others. The results also suggest that Ag nanoparticles might affect the development of embryos stochastically due to the random diffusion of nanoparticles.

As nanoparticle concentration increases, the number of normally developed zebrafish decreases, while the number of dead zebrafish increases (Fig. 7A: a). As nanoparticle concentration increases beyond 0.19 nM, only dead and deformed zebrafish are observed, showing a critical concentration of Ag nanoparticles on the development of zebrafish embryos (Fig. 7A). The blank (negative) control experiments, conducted by replacing nanoparticles with the supernatant resulting from washing Ag nanoparticles, show that the survival rate of zebrafish is independent of the dose of supernatant (Fig. 7A: b), demonstrating that residual chemicals from nanoparticle synthesis are not responsible for the deformation and death of zebrafish, but rather the nanoparticles that were used to treat the zebrafish embryos (Fig. 7A: a).

The number of deformed zebrafish increased to its maximum as nanoparticle concentration increased to 0.19 nM, and then decreased as nanoparticle concentration increased from 0.19 to 0.71 nM (Fig. 7A: c) because the number of dead zebrafish increased. Interestingly, the types of viable deformities exhibit high dependence on the nanoparticle concentration (Fig. 7A: d).

For example, the fanfold abnormality and tail/spinal cord flexure and truncation were observed in zebrafish treated with all tested nanoparticle concentrations (0.04–0.71 nM) with the highest occurrences at 0.19 and 0.38 nM, respectively. Cardiac malformation and yolk sac edema were observed in zebrafish treated with the slightly higher nanoparticle concentrations (0.07–0.71 nM) with the highest occurrences at 0.66 nM. In contrast, head edema and eye deformity were only observed in the higher concentrations of nanoparticles, 0.44–0.71 and 0.66–0.71 nM, respectively. Among all types of observed deformities, finfold abnormality occurred at the highest rate, followed by tail and spinal cord flexure and truncation, then cardiac malformation and yolk sac edema, and finally head edema and eye abnormality, which were rarely observed deformations of zebrafish and quickly led to zebrafish death.

Representative deformed zebrafish induced by nanoparticles are illustrated in Fig. 7B:b–g and summarized in on-line supporting information (SI). In comparison with the normally developed zebrafish in Fig. 7B-a, we found characteristics of finfold abnormality (Fig. 7B-b), tail and spinal cord flexure and truncation (Fig. 7B-c), cardiac malformation (Fig. 7B-d), yolk sac edema (Fig. 7B-e), head edema (Fig. 7B-f), and eye abnormality (Fig. 7B-g) of zebrafish that developed from the 8-cell embryos treated chronically by Ag nanoparticles. Interestingly, multiple deformities occurred in one zebrafish at the higher nanoparticle concentrations (> 0.38 nM). For example, in yolk sac edema zebrafish, we also observed tail/spinal cord flexure, finfold abnormality, and cardiac malformation (Fig. 7B: c-iv & e-ii), head edema (Fig 7B: e-ii, e-iv and f-ii), and eye abnormality (Fig 7B: g-i). These findings suggest that specific embryonic developmental pathways might be co-regulated, and that some deformities (e.g., finfold, tail, spinal cord) are much more sensitive to the nanoparticles than others (e.g., head edema, eye abnormality).

To determine the possible targets for further genomic and proteomic studies and evaluate the toxicity of Ag nanoparticles against well-studied toxic chemicals, such as cadmium, dichloroacetic acid (DCA), 2,3,7,8-tetrachlorodibenzo-p-dioxin (TCDD), and ethanol, we compare the characteristics of deformation of zebrafish induced by Ag nanoparticles with those generated by well-known toxic chemicals. We found that the observed finfold abnormality and tail/spinal cord flexure and truncation induced by Ag nanoparticles (Fig. 7B: b & c) are similar to those treated by DCA and cadmium[32, 33], indicating possible common targets of malformation during development. The observed cardiac malformation and yolk sac edema in this study (Fig. 7B: d & e) are also similar to those treated with DCA and cadmium.[32, 33] The shrunken ventricular myocardium observed in cardiac malformed zebrafish induced by nanoparticles (Fig. 7B: d) is similar to those treated with TCDD.[34] Head edema and eye abnormality in Fig. 7B: f & g-i have also been found in treatment of zebrafish with cadmium.[32]

Although the eye malformation (a cycloptic eye development) had been observed in zebrafish treated by ethanol,[35] the deformation is unlike what we have observed (eyeless, no formation of retina or lens) in Fig. 7B: g-ii. Thus, the eyeless deformation (Fig. 7B: g-ii), an undeveloped set of optic cups with no retina or eye lens, to our knowledge, is a new occurrence of malformation that has not been reported previously. This abnormality may be related to the nanoparticles disrupting the regulators or signaling cascades involved with the normal development of the neural retinal layers and the lens of the zebrafish's eye. A transcription factor, Pax-6, has been studied and shown to affect the development of the eye retinal layers. In Pax-6 mutants, the lens fails to develop.[35, 36] However, another transcription factor, Six-6, regulating neural retinal development in zebrafish has not been studied in detail and it may also play the role in eye deformation as well.[36] Further studies are needed to determine whether Ag nanoparticles inhibit or regulate the expression of transcription factors (e.g., Pax-6 and Six-6), leading to the eyeless deformation.

Plausible explanations for the high dependence of embryonic abnormalities on the dose of nanoparticles include the following: (i) The rate of passive diffusion (permeability) and accumulation of nanoparticles in chorion pore canals and embryos highly depends on the concentration gradient of nanoparticles. Thus, the dose of nanoparticles plays a vital role in determining the rate and amount of nanoparticles that can penetrate into particular compartments of embryos, and the rate and number of chorion pore canals blocked by the aggregation of nanoparticles (Fig. 3–Fig. 5). (ii) The accumulated nanoparticles inside embryos can also alter the charge, diffusion, and interactions of biomolecules (e.g., nucleic acids, proteins such as transcription factors, signaling molecules) in a dose-dependent manner, leading to interference or malfunctioning of signaling cascades.

Taken together, these results suggest that specific pathways of embryonic development respond to Ag nanoparticles in a dose dependent manner, and demonstrate that the nanoparticles may elicit unique response from embryonic neural development pathways. The study demonstrates the possibility of fine-tuning the dose of nanoparticles to (i) selectively target specific pathways to create particular phenotypes, (ii) selectively generate specific mutations in zebrafish, and (iii) serve as potential therapeutic agents to treat specific disorders in embryonic development. Unlike other chemicals, single nanoparticles can be traced and imaged inside developing embryos and developed zebrafish with nanometer spatial resolution in real-time, offering new opportunities to unravel the related pathways that lead to the abnormalities. Work is in progress to identify the related specific pathways and signaling cascades at the genomic and proteomic levels and to further explore potential therapeutic effects of nanoparticles.

Summary

In summary, we have designed, synthesized and characterized single nanoparticle optical probes (individual Ag nanoparticles) for probing their transport, biocompatibility and toxicity in early development of zebrafish embryos in real-time. We have shown that single Ag nanoparticles resist photodecomposition and blinking and can be directly monitored in embryos for an extended period of time. Furthermore, individual Ag nanoparticles exhibit size-dependent LSPR spectrum (color), which permits us (i) to distinguish them from tissue debris and vesicles in embryos, (ii) to directly image and characterize the sizes of individual nanoparticles in solution and in living embryos in real time, (iii) to probe their diffusion, transport mechanism and biocompatibility in living embryos in real time, and (iv) to investigate the embryonic fluids (e.g., viscosity) at nm spatial resolution in real time. We found that individual Ag nanoparticles can passively diffuse into developing embryos via chorion pore canals, create specific effects on embryonic development and selectively generate particular phenotypes in a dose-dependent manner. The early embryos are highly sensitive to the nanoparticles, showing the possibility of using zebrafish embryos as an *in vivo* assay to screen the biocompatibility and toxicity of nanomaterials. This study represents the first direct observation of passive diffusion of nanoparticles into an *in vivo* system (an important aquatic species), suggesting that the release of large amounts of Ag nanoparticles into aquatic ecosystems (e.g., rivers) may have drastic environmental consequences, should the sizes of nanomaterials remain unchanged during environmental transport. This study also represents the first most rigorous study and characterization of nano-toxicity and nano-biocompatibility ever performed by investigating the effect of highly purified nanoparticles *in vivo* in real time and considering the effect of possible trace chemicals from nanoparticle synthesis.

Methods

Synthesis and characterization of silver (Ag) nanoparticles

Silver nanoparticles were synthesized by reducing a 0.1 mM silver perchlorate solution with a freshly prepared ice-cold solution of 3 mM sodium citrate and 10 mM sodium borohydride

under stirring overnight, and filtered through a 0.22 μm filter.[11, 37] The nanoparticles were washed twice with nanopure water using centrifugation to remove the chemicals involved in nanoparticle synthesis, and the nanoparticle pellets were resuspended in nanopure water before incubating with embryos. The washed Ag nanoparticles are very stable (non-aggregated) in nanopure water for months and remain stable in egg water throughout the entire experiments (120 hpf). The supernatants of nanoparticle solutions after the second washing were collected for control experiments to study the effect of trace chemicals involved in nanoparticle synthesis on the development of embryos. The concentration, optical properties, and size of nanoparticles were characterized using UV-vis spectroscopy, dark-field single nanoparticle optical microscopy and spectroscopy (SNOMS)[10–12], high-resolution transmission electron microscopy (HR-TEM) (FEI Tecnai G2 F30 FEG), and dynamic light scattering (DLS) (Nicomp 380ZLS particle sizing system), respectively. Our dark-field SNOMS has been well described previously for real-time imaging and spectroscopic characterization of single nanoparticles in single living cells and for single molecule detection.[10–12, 31, 38, 39] The detector, EMCCD or LN back-illuminated CCD camera coupled with a SpectraPro-150 (Roper Scientific), was used in this study. All chemicals were purchased from Sigma and used without further purification or treatment.

To determine the photostability of single Ag nanoparticles, we acquired sequence images of single Ag nanoparticles using EMCCD camera with exposure time at 100 ms and readout time of 40.6 ms while these nanoparticles were constantly radiated under dark-field microscope illuminator (100 W halogen) for 12 hr. The illumination power at the sample stage (focal plane of dark field) is 0.070 ± 0.001 Watt. The integrated scattering intensity of single nanoparticles and background (in the absence of nanoparticles) within a 20×20 CCD pixel area was measured. The integrated scattering intensity of background is subtracted from that of same size of detection area in the presence of individual nanoparticles to calculate the scattering intensity of single nanoparticles. The experiments were repeated at least three times. The average subtracted integrated intensity of the single nanoparticles and background was plotted as a function of time (Fig. 1F). The fluctuations of intensity of single nanoparticles were used to compare with those of background to determine the photostability (photodecomposition and blinking) of single nanoparticles.

Breeding and monitoring of zebrafish embryos

Wildtype adult zebrafish (Aquatic Ecosystems) were maintained, bred, and collected, as described previously.[40] Embryos were collected and transferred into a petri dish containing egg water (1.2 mM stock salts in DI water), washed twice with egg water to remove the surrounding debris, and placed into 24-well plates with each well containing two embryos in egg water. Each developmental stage of embryos in the wells was directly imaged by bright-field optical microscopy using an inverted microscope equipped with a 4x objective and a digital camera.

In vivo characterization and analysis of transport and dose-dependent biocompatibility and toxicity of nanoparticles

Cleavage-stage living embryos (8–64 cell stage; 0.75–2.25 hpf) that had been incubated with 0.19 nM nanoparticles for a given time (0–2 hours) were either immediately imaged to investigate the transport of nanoparticles into embryos or carefully rinsed with DI water to remove external nanoparticles, and placed in a self-made microwell containing DI water to image the diffusion and transport of nanoparticles inside the embryos in real-time using our SNOMS.

To study the dose-dependent effects of nanoparticles on embryonic development, a dilution series of washed Ag nanoparticle solutions (0, 0.04, 0.06, 0.07, 0.08, 0.19, 0.38, 0.57, 0.66,

and 0.71 nM) were incubated chronically with cleavage (8-cell) stage embryos in egg water for 120 hpf. Each experiment was carried out at least three times and total number of embryos at 35–40 was studied for each individual concentration to gain representative statistics. Nanoparticle concentrations were calculated as described previously.[41] Embryos in egg water in the absence of nanoparticles and in the presence of supernatant were placed in two rows of the 24-well plates as control experiments of untreated embryos and probing the effect of possible trace chemicals from nanoparticle synthesis, respectively. The embryos in the 24-well plates were incubated at 28.5°C, and directly observed at room temperature using an inverted microscope equipped with a digital camera at 24, 48, 72, 96, and 120 hpf.

Characterization of nanoparticles embedded inside embryos and fully developed zebrafish

To characterize the embedded nanoparticles in the tissues of treated zebrafish, we selected living developed zebrafish that had been chronically incubated with a given concentration (0.04 nM) of nanoparticles for 120 hpf since their cleavage (8-cell) stage, and carefully rinsed the zebrafish with DI water to remove external nanoparticles. The fixed zebrafish were prepared using 10% buffered formalin via a standard histology protocol of tissue sample preparation.[42] The thin-layer microsections (~5 μm thickness) of its tissues were prepared by carefully dissecting the tissues of interest (e.g., eye retina, brain, heart, gill arch, tail and spinal cord) under microscopy using microtome. The embedded nanoparticles in the tissues were directly characterized using SNOMS (Fig. 6).

Supplementary Material

Refer to Web version on PubMed Central for supplementary material.

Acknowledgements

We thank E. Dupont for her helpful assistance in literature search and CharFac of University of Minnesota (a NNIN site funded by NSF) for their assistance to characterize Ag nanoparticles using HRTEM. This work is supported in part by NSF (NIRT: BES 0507036) and NIH (R01 GM0764401). Lee, Nallathamby, Browning, and Dupont are grateful for the support of NSF-GRAS (BES 0541661), Dominion Scholar Fellowship, NIH-GRAS (R01 GM076440-01S1), and NSF-RETS (BES 0507036), respectively.

References

1. Tiwari SB, Amiji MM. A Review of Nanocarrier-Based CNS Delivery Systems. Curr. Drug Deliv 2006;3(2):219–232. [PubMed: 16611008]
2. Xu, XHN.; Patel, RP. Nanoparticles for Live Cell Dynamics. In: Nalwa, HS., editor. Encyclopedia of Nanoscience and Nanotechnology. Vol. Vol. 7. American Scientific Publishers; 2004. p. 189-192.
3. Xu, XHN.; Patel, RP. Imaging and Assembly of Nanoparticles in Biological Systems. In: Nalwa, HS., editor. Handbook of Nanostructured Biomaterials and Their Applications in Nanobiotechnology. Vol. Vol. 1. American Scientific Publishers; 2005. p. 435-456.
4. Xu, XHN.; Song, Y.; Nallathamby, PD. Probing Membrane Transport of Single Live Cells Using Single Molecule Detection and Single Nanoparticle Assay. In: Xu, XHN., editor. New Frontiers in Ultrasensitive Bioanalysis: Advanced Analytical Chemistry Applications in Nanobiotechnology, Single Molecule Detection, and Single Cell Analysis. New Jersey: Wiley; 2007. p. 41-65.
5. Yamada T, Iwasaki Y, Tada H, Iwabuki H, Chuak MKI, VandenDriessche T, Fukuda H, Kondo A, Ueda M, Seno M, Tanizawa K, Kuroda S. Nanoparticles for the Delivery of Genes and Drugs to Human Hepatocytes. Nature Biotechnology 2003;21:885–890.
6. Nel A, Xia T, Madler L, Li N. Toxic Potential of Materials at the Nanolevel. Science 2006;311:622–627. [PubMed: 16456071]
7. Agrawal A, Zhang C, Byassee T, Tripp RA, Nie S. Counting Single Native Biomolecules and Intact Viruses with Color-Coded Nanoparticles. Anal. Chem 2006;78:1061–1070. [PubMed: 16478096]

8. Bruchez M Jr, Moronne M, Gin P, Weiss S, Alivisatos AP. Semiconductor Nanocrystals as Fluorescent Biological Labels. Science 1998;281:2013–2016. [PubMed: 9748157]
9. Chan WC, Nie S. Quantum Dot Bioconjugates for Ultrasensitive Nonisotopic Detection. Science 1998;281:2016–2018. [PubMed: 9748158]
10. Kyriacou S, Brownlow W, Xu X-HN. Nanoparticle Optics for Direct Observation of Functions of Antimicrobial Agents in Single Live Bacterial Cells. Biochemistry 2004;43:140–147. [PubMed: 14705939]
11. Xu XHN, Brownlow WJ, Kyriacou SV, Wan Q, Viola JJ. Real-Time Probing of Membrane Transport in Living Microbial Cells Using Single Nanoparticle Optics and Living Cell Imaging. Biochemistry 2004;43:10400–10413. [PubMed: 15301539]
12. Xu XHN, Chen J, Jeffers RB, Kyriacou SV. Direct Measurement of Sizes and Dynamics of Single Living Membrane Transporters Using Nano-Optics. Nano Lett 2002;2:175–182.
13. Alivisatos AP. Perspectives on the Physical Chemistry of Semiconductor Nanocrystals. J. Phys. Chem. B 1996;100:13226–13239.
14. Bohren, CF.; Huffman, DR. Absorption and Scattering of Light by Small Particles. New York, NY: Wiley; 1983. p. 287-380.
15. Kreibig, U.; Vollme, M. Optical Properties of Metal Clusters. Berlin: Springer; 1995. p. 14-123.
16. Mie G. Beiträg Zur Optik Trüber Medien, Speziell Kolloidaler Metrallősungen. Ann. Phys 1908;25:377–445.
17. Mulvaney P. Surface Plasmon Spectroscopy of Nanosized Metal Particles. Langmuir 1996;12:788–800.
18. den Hertog J. Chemical Genetics: Drug Screens in Zebrafish. Biosci. Rep 2005;25:289–297. [PubMed: 16307377]
19. Hill AJ, Teraoka H, Heideman W, Peterson RE. Zebrafish as a Model Vertebrate for Investigating Chemical Toxicity. Toxicol. Sci 2005;86(1):6–19. [PubMed: 15703261]
20. Kahn P. Zebrafish Hit the Big Time. Science 1994;264:904–905. [PubMed: 8178149]
21. Teraoka H, Dong W, Hiraga T. Zebrafish as a Novel Experimental Model for Developmental Toxicology. Congenit. Anom. (Kyoto) 2003;43:123–132. [PubMed: 12893971]
22. Zon LI, Peterson RT. In Vivo Drug Discovery in the Zebrafish. Nat. Rev. Drug Discov 2005;4:35–44. [PubMed: 15688071]
23. Rieger S, Kulkarni RP, Darcy D, Fraser SE, Koster RW. Quantum Dots Are Powerful Multipurpose Vital Labeling Agents in Zebrafish Embryos. Dev. Dyn 2005;234:670–681. [PubMed: 16110511]
24. Luckenbill-edds L. Introduction: Research News in Developmental Biology in 1895 and 1995. Amer. Zool 1997;37:213–219.
25. Strehlow D, Heinrich G, Gilbert W. The Fates of the Blastomeres of the 16-Cell Zebrafish Embryo. Development 1994;120:1791–1798. [PubMed: 7924986]
26. Hoar, WS.; Randall, DJ. Fish Physiology: The Physiology of Developing Fish, Part A, Eggs and Larvae. New York, NY: Academic Press; 1988. p. 253-255.
27. Rawson DM, Zhang T, Kalicharan D, Jongebloed WL. Field Emission Scanning Electron Microscopy and Transmission Electron Microscopy Studies of the Chorion, Plasma Membrane and Syncytial Layers of the Gastrula Stage Embryo of the Zebrafish Brachydanio Rerio: A Consideration of the Structural and Functional Relationships with Respect to Cryoprotectant Penetration. Aquaculture Research 2000;31:325–336.
28. Kusumi A, Sako Y. Compartmental Structure of the Plasma Membrane for Receptor Movements as Revealed by a Nanometer-Level Motion Analysis. J Cell Biol 1994;125:1251–1264. [PubMed: 8207056]
29. Kusumi A, Sako Y, Yamamoto M. Confined Lateral Diffusion of Membrane Receptors as Studied by Single Particle Tracking (Nanovid Microscopy). Effects of Calcium-Induced Differentiation in Cultured Epithelial Cells. Biophys. J 1993;65:2021–2040. [PubMed: 8298032]
30. Tinoco, I.; Sauer, K.; Wang, J.; Puglisi, JD. Physical Chemistry-Principles and Applications in Biological Sciences. Prentice Hall; 2002. Molecular Motion and Transport Properties; p. 274-290.
31. Xu XHN, Jeffers RB, Gao J, Logan B. Novel Solution-Phase Immunoassays for Molecular Analysis of Tumor Markers. Analyst 2001;126:1285–1292. [PubMed: 11534594]

32. Hallare AV, Schirlinga M, Luckenbacha T, Kohler H-R, Triebskorn R. Combined Effects of Temperature and Cadmium on Developmental Parameters and Biomarker Responses in Zebrafish (Danio Rerio) Embryos. J. Thermal Biology 2005;30:7–17.
33. Williams FE, Sickelbaugh TJ, Hassoun E. Modulation by Ellagic Acid of DCA-Induced Developmental Toxicity in the Zebrafish (*Danio Rerio*). J. Biochem. Mol. Toxicol 2006;20:183–190. [PubMed: 16906523]
34. Antkiewicz DS, Burns CG, Carney SA, Peterson RE, Heideman W. Heart Malformation Is an Early Response to TCDD in Embryonic Zebrafish. Toxicol. Sci 2005;84:368–377. [PubMed: 15635151]
35. Arenzana FJ, Carvan MJ 3rd, Aijon J, Sanchez-Gonzalez R, Arevalo R, Porteros A. Teratogenic Effects of Ethanol Exposure on Zebrafish Visual System Development. Neurotoxicol. Teratol 2006;28:342–348. [PubMed: 16574376]
36. Jean D, Ewan K, Gruss P. Molecular Regulators Involved in Vertebrate Eye Development. Mech. Dev 1998;76:3–18. [PubMed: 9767078]
37. Lee PC, Meisel D. Adsorption and Surface-Enhanced Raman of Dyes on Silver and Gold Sols. J. Phys. Chem. B 1982;86:3391–3395.
38. Kyriacou SV, Nowak ME, Brownlow WJ, Xu XHN. Single Live Cell Imaging for Real-Time Monitoring of Resistance Mechanism in *Pseudomonas Aeruginosa*. J. Biomed. Opt 2002;7:576–586. [PubMed: 12421124]
39. Xu XHN, Brownlow WJ, Huang S, Chen J. Real-Time Measurements of Single Membrane Pump Efficiency of Single Living Pseudomonas Aeruginosa Cells Using Fluorescence Microscopy and Spectroscopy. Biochem. Biophys. Res. Commun 2003;305:79–86. [PubMed: 12732199]
40. Westerfield, M. The zebrafish book: A Guide for the Laboratory Use of Zebrafish (Danio Rerio*). Eugene, OR: University of Oregon Press; 1993. http://zfin.org/zf_info/zfbook/zfbk.html
41. Xu X-HN, Huang S, Brownlow W, Salatia K, Jeffers R. Size and temperature dependence of surface plasmon absorption of gold nanoparticles induced by Tris(2,2'-bipyridine)ruthenium(II). J. Phys. Chem. B 2004;108:15543–15551.
42. Mohideen M-APK, Beckwith LG, Tsao-Wu GS, Moore JL, Wong ACC, Chinoy MR, Cheng KC. Histology-Based Screen for Zebrafish Mutants with Abnormal Cell Differentiation. Developmental Dynamics 2003;228:414–423. [PubMed: 14579380]

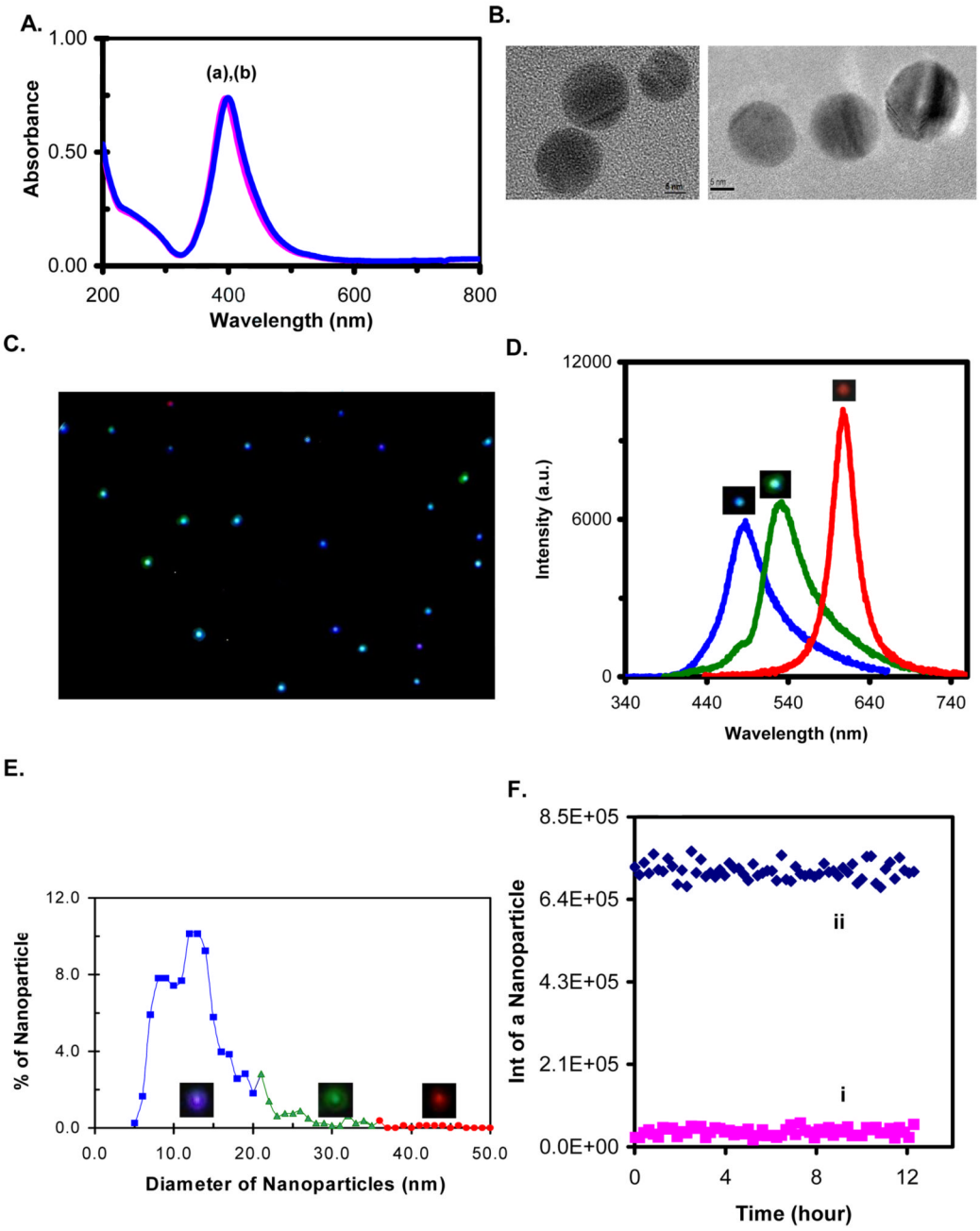

Figure 1. Characterization of optical properties and stability of Ag nanoparticles

(A) Representative UV-vis absorption spectra of 0.71 nM Ag nanoparticles well-dispersed in egg water at 28°C for (i) 0 and (ii) 120 hours show that the peak absorbance and wavelength at 396 nm remain unchanged for 120 hours;

(B) Representative HR-TEM images of Ag nanoparticles show the size and spherical shape of single Ag nanoparticles. Scale bar = 5 nm;

(C) Representative dark-field optical image of single Ag nanoparticles shows the majority of nanoparticles are blue with some being green and few are red;

(D) Representative LSPR spectra (color) of single Ag nanoparticles exhibit peak wavelength at 452, 531, and 601 nm, respectively;

(E) Histogram of size and color distribution of individual Ag nanoparticles shows the average size of nanoparticles to be 11.6 ± 3.5 nm, with 74% of 5–15 nm (blue), 23% of 16–30 nm (green), and 1% of 31–46 nm (red) Ag nanoparticles;
(F) Representative plots of scattering intensity of single nanoparticles (i) and background (ii) versus illumination time show that single Ag nanoparticles resist photobleaching and blinking.

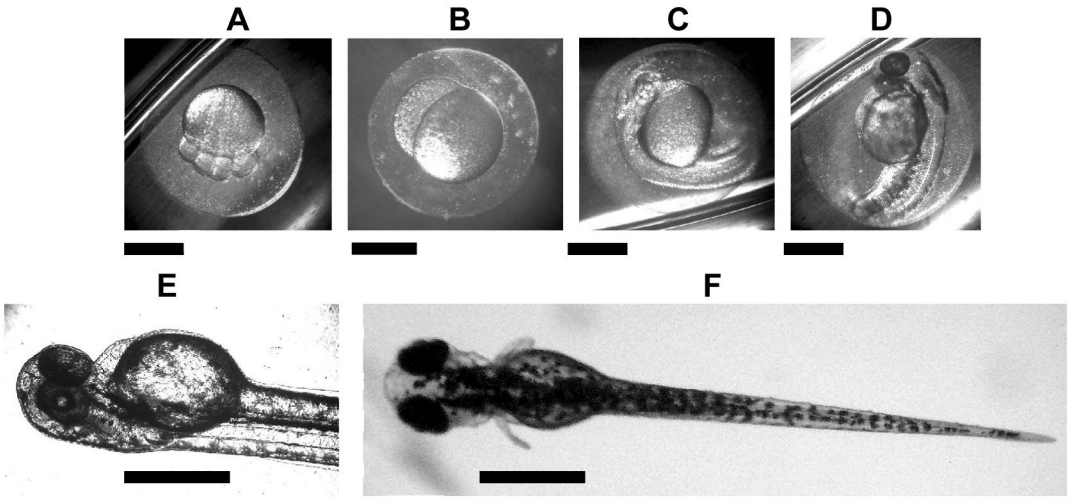

Figure 2.
Optical images of the representative developmental stages of normally developed zebrafish in egg water (in the absence of nanoparticles) show an embryo at (A) 1.25–1.50 hpf (8-cell stage); (B) 2–2.25 hpf (64-cell stage); (C) 24 hpf (segmentation stage); (D) 48 hpf (hatching stage); (E) 72 hpf (pharyngula stage); and (F) a completely developed zebrafish at 120 hpf. Scale bar = 500 μm. hpf = hour post fertilization.

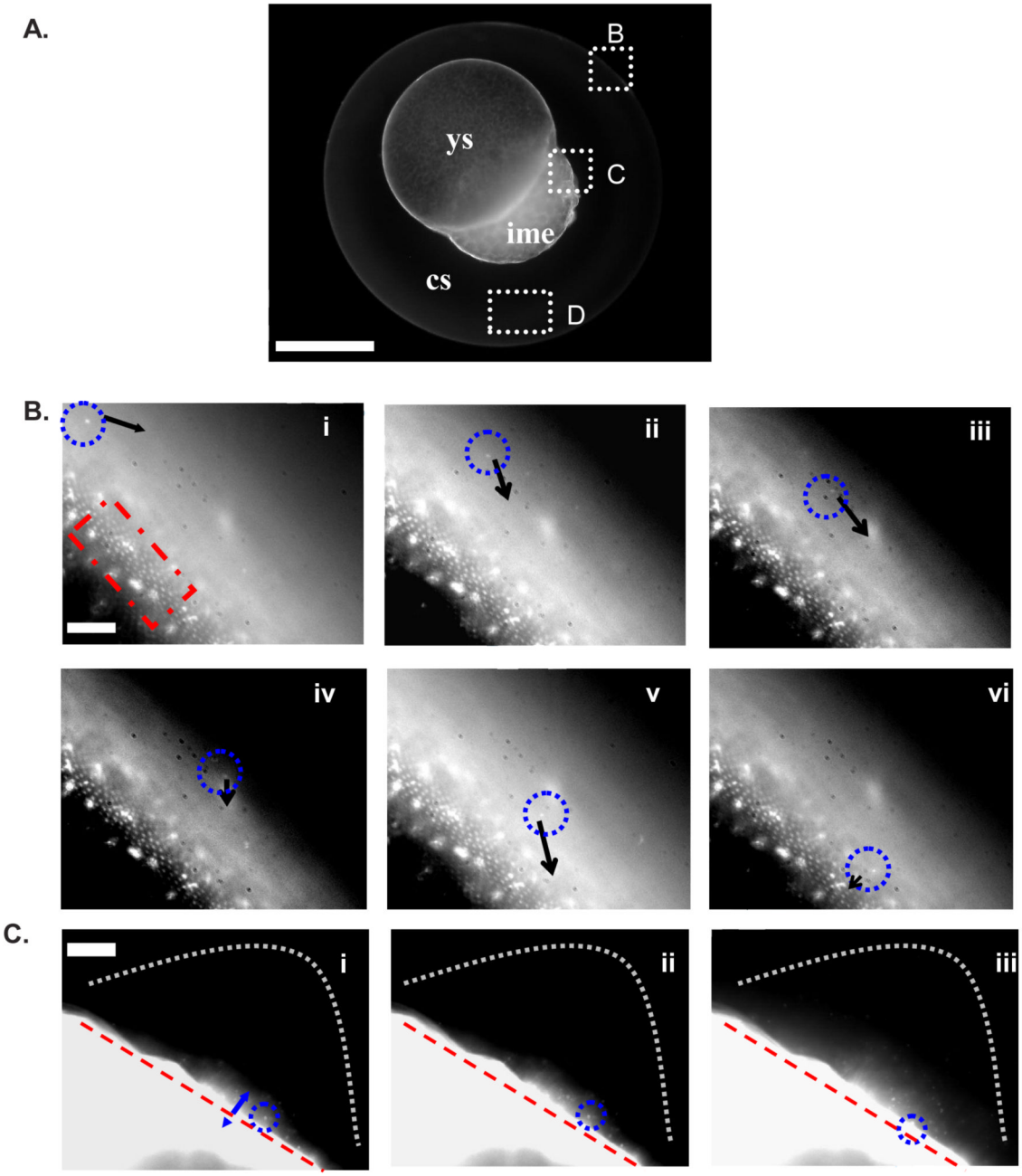

Figure 3. Real-time monitoring and characterization of transport of individual Ag nanoparticles in a cleavage-stage living embryo (64-cell stage; 2–2.25 hpf)

(A) Optical image of a cleavage-stage embryo shows chorionic space (cs), yolk sac (ys), and inner mass of embryo (ime). The transport of single Ag nanoparticles at the interface of egg water with chorionic space, interface of chorionic space with inner mass of embryo, and inside chorionic space, as marked by B, C and D, are shown in Movie 1–Movie 3 of online supporting information (SI), respectively. The snap shots of transport of single nanoparticles at the interfaces of egg water/chorionic space and chorionic space/ inner mass of embryo are illustrated in (B) and (C). LSPR spectra (color) of individual nanoparticles were used to distinguish them from tissue debris or vesicles in embryos.

(B) Sequence dark-field optical images illustrate the transport of single Ag nanoparticles, as indicated by the circle, from the egg water (extra embryo) into the chorionic space via an array of chorion pore canals (CPCs) highlighted by a rectangle.
(C) Sequence dark-field optical images illustrate the transport of single Ag nanoparticles, as indicated by the circle, from chorionic space into inner mass of embryo. The straight and curved dashed-lines illustrate the interface of inner mass of embryo with chorionic space, and chorionic space with egg water, respectively.
The time interval of each sequence image in both (B) and (C) is 25 s. Scale bar = 400 μm in (A) and 15 μm in (B–C).

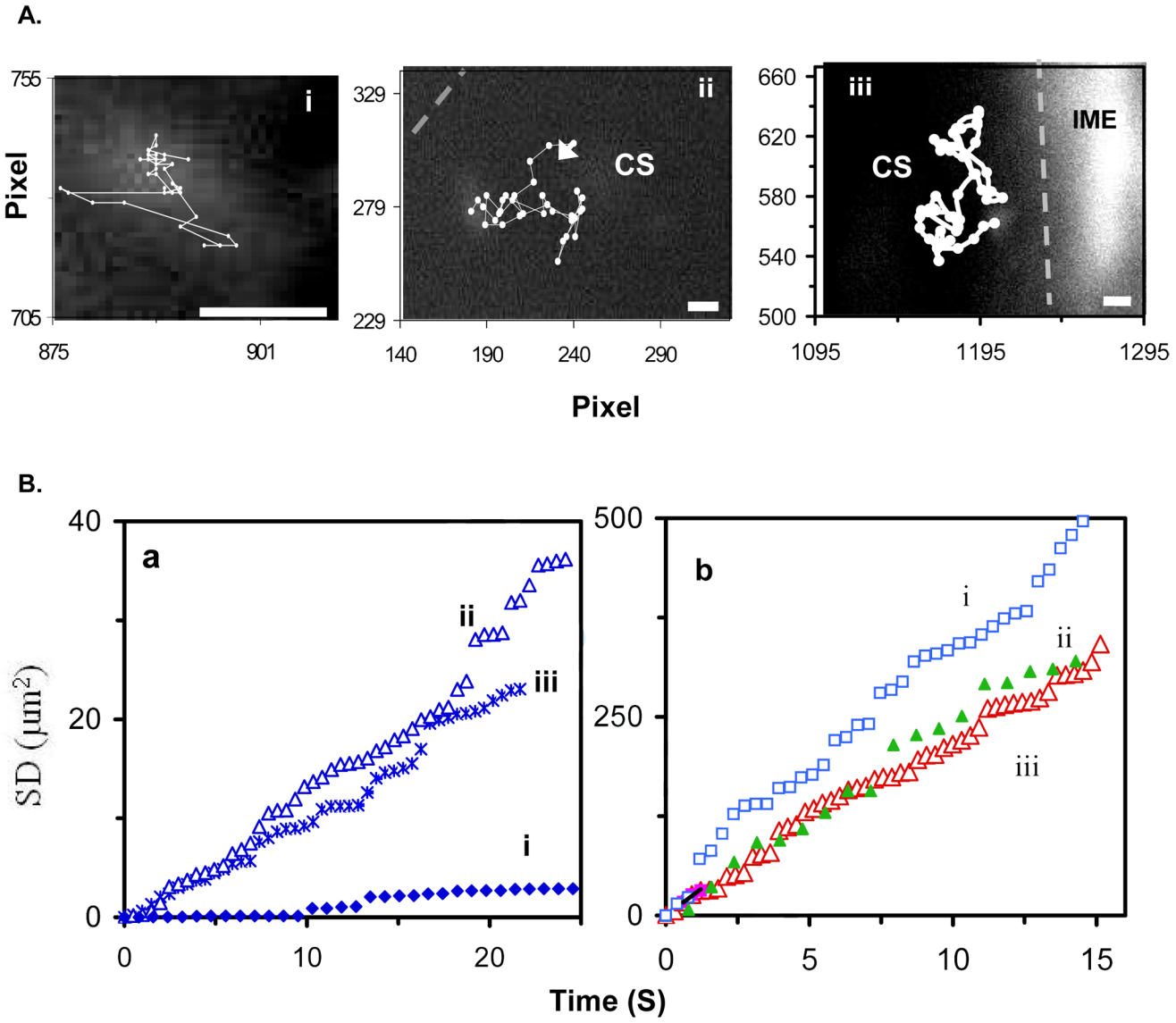

Figure 4. Characterization of transport and diffusion of single Ag nanoparticles in a cleavage (64-cell) stage living embryo

(A) Diffusion trajectories of single Ag nanoparticles: (i) a red nanoparticle inside the chorion layers, (ii) a blue nanoparticle inside chorionic space, and (iii) a green nanoparticle at the interface of inner mass of embryo and chorionic space. Their real-time videos are shown in SI (Movie 3–Movie 4).

(B) Plots of real-time square-displacement (RTSD) as a function of time:

(a) single nanoparticles from the diffusion trajectories shown in A (i–iii) illustrate that (i) a red nanoparticle in a restricted and stationary diffusion mode with a diffusion coefficient (D) < 1.9×10^{-11} cm^2/s, due to entrapment inside chorion pore canals; (ii) a blue nanoparticle in chorionic space away from the inner mass of embryo; and (iii) a green nanoparticle inside chorionic space near the surface of inner mass of embryo, both in a simple Brownian motion with D of 3.4×10^{-9} cm^2/s and 2.6×10^{-9} cm^2/s, respectively;

(b) a representative single (i) blue, (ii) green and (iii) red nanoparticle in egg water. All show simple Brownian diffusion with D of 8.4 $\times10^{-8}$, 6.0 $\times10^{-8}$ and 5.5 $\times10^{-8}$ cm^2/s, respectively.

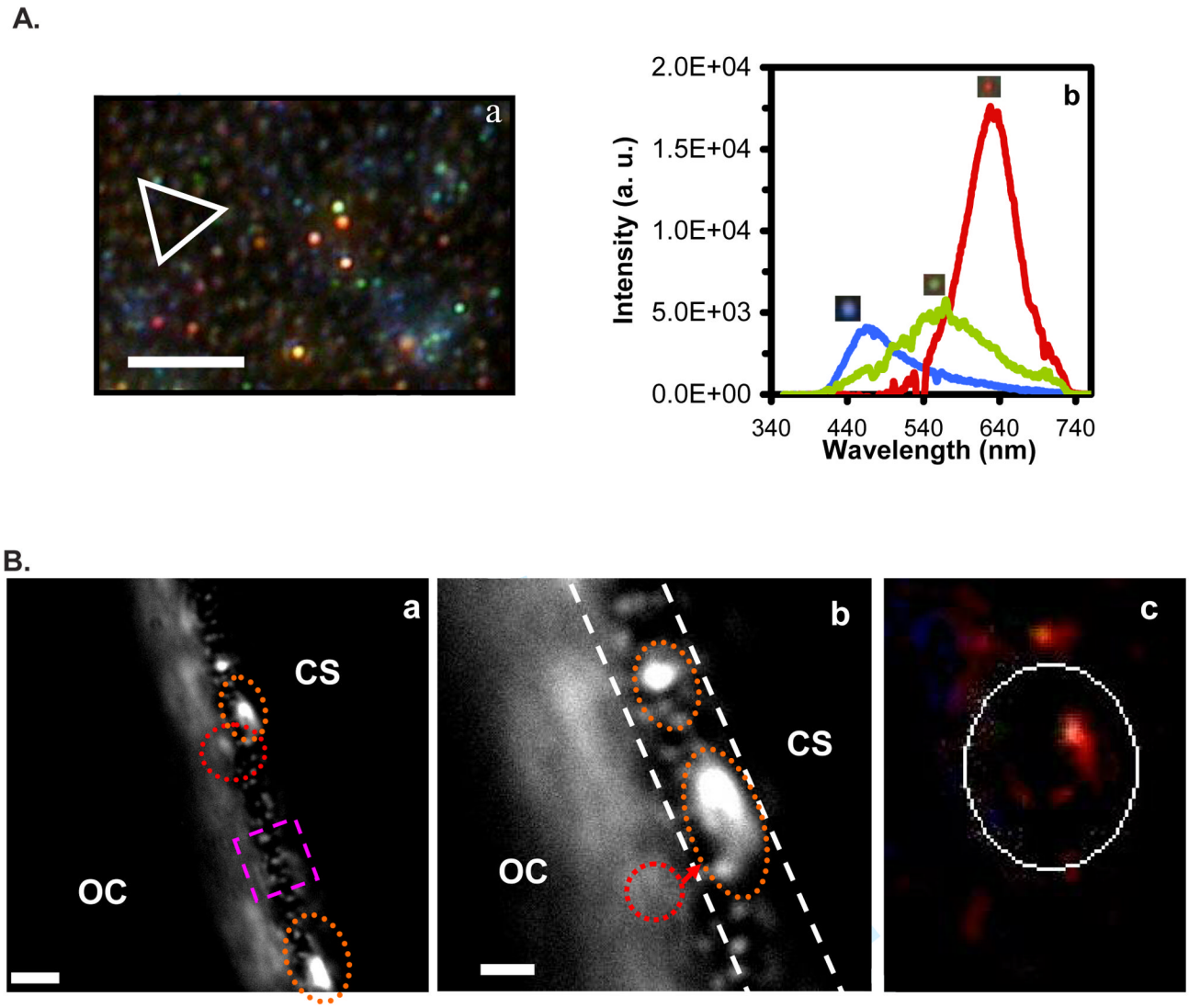

Figure 5. Characterization of Ag nanoparticles embedded in embryos using dark-field SNOMS

(A) Representative (a) color image and (b) LSPR spectra of single Ag nanoparticles embedded in chorion layers show that single Ag nanoparticles with multiple-colors (blue, green, red) are present inside chorion layers, and some nanoparticles are overlapped with the chorion pore canals (note that an array of chorion pore canals are highlighted by a triangle). Scale bar = 1 μm

(B) Representative images of individual Ag nanoparticles embedded in the chorion layers illustrate those Ag nanoparticles (as indicated by a circle) trapped in the chorion pore canals outlined by ellipses. The CCD image in (a) is enlarged and shown in (b). The zoom-in color image of (b) is shown in (c), indicating that the dark-red nanoparticles clog the chorion pore canals. Scale bar = 10 μm in (a); 2 μm in (b). OC = outside chorion

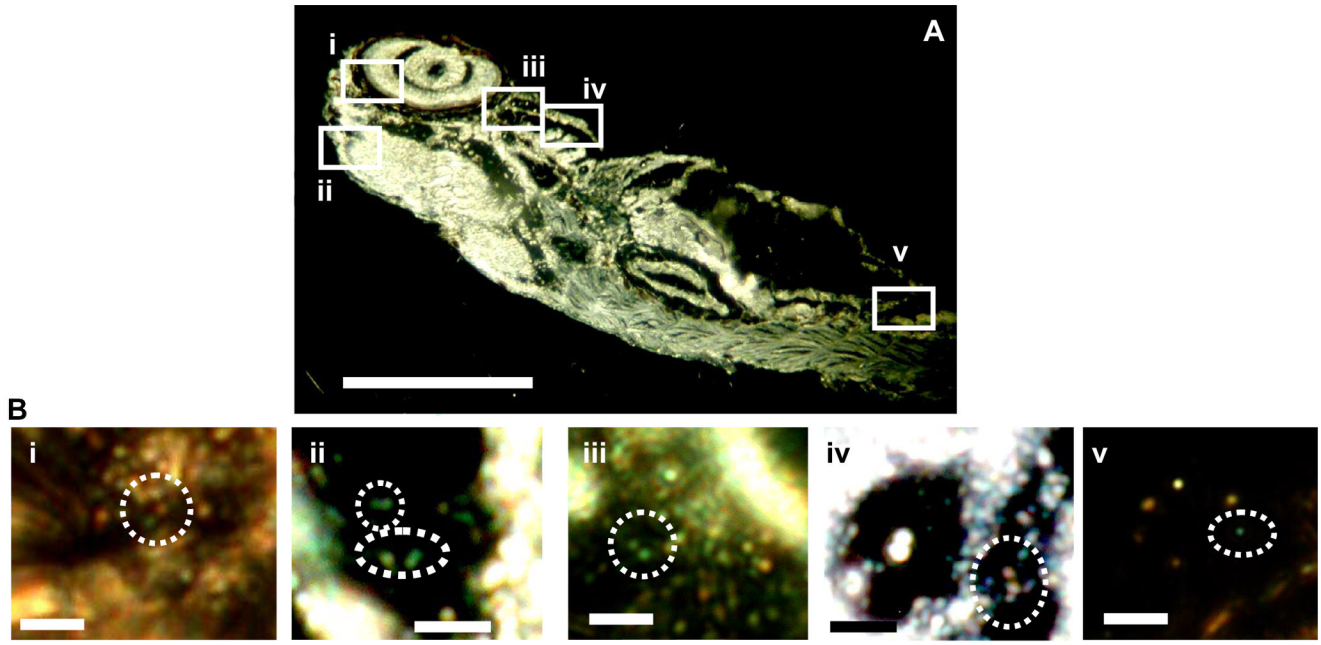

Figure 6. Characterization of individual Ag nanoparticles embedded inside a fully developed (120 hpf) zebrafish using dark-field SNOMS

(A) optical image of a fixed normally developed zebrafish. The rectangles (i–v) highlight representative areas: (i) retina, (ii) brain (mesencephalon cavity), (iii) heart, (iv) gill arches, and (v) tail.

(B) Zoom-in optical images of single Ag nanoparticles embedded in those tissue sections outlined in (A). Dashed circles outline the representative embedded individual Ag nanoparticles. Scale bar = 400 μm in (a); 4 μm in (b).

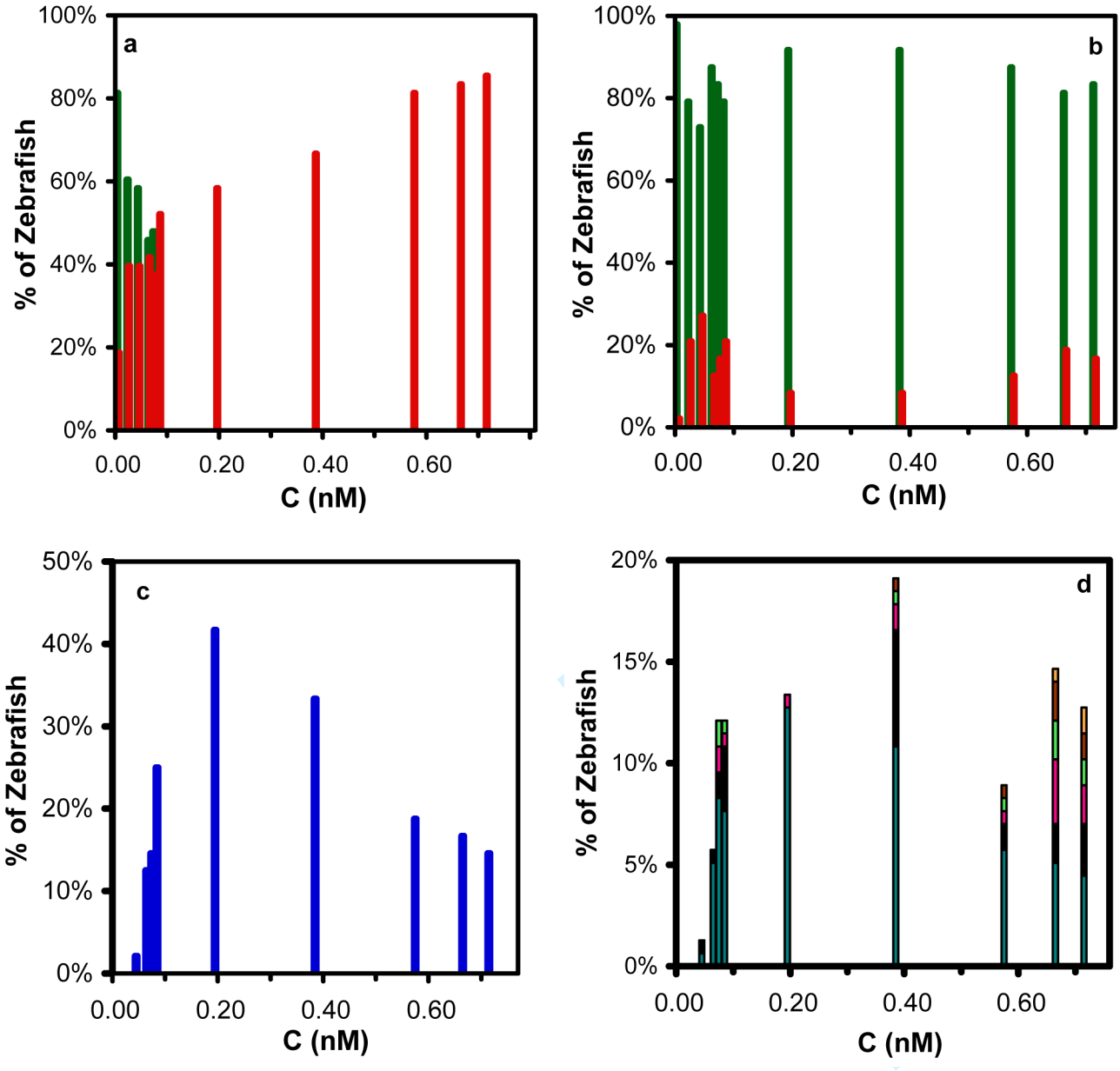

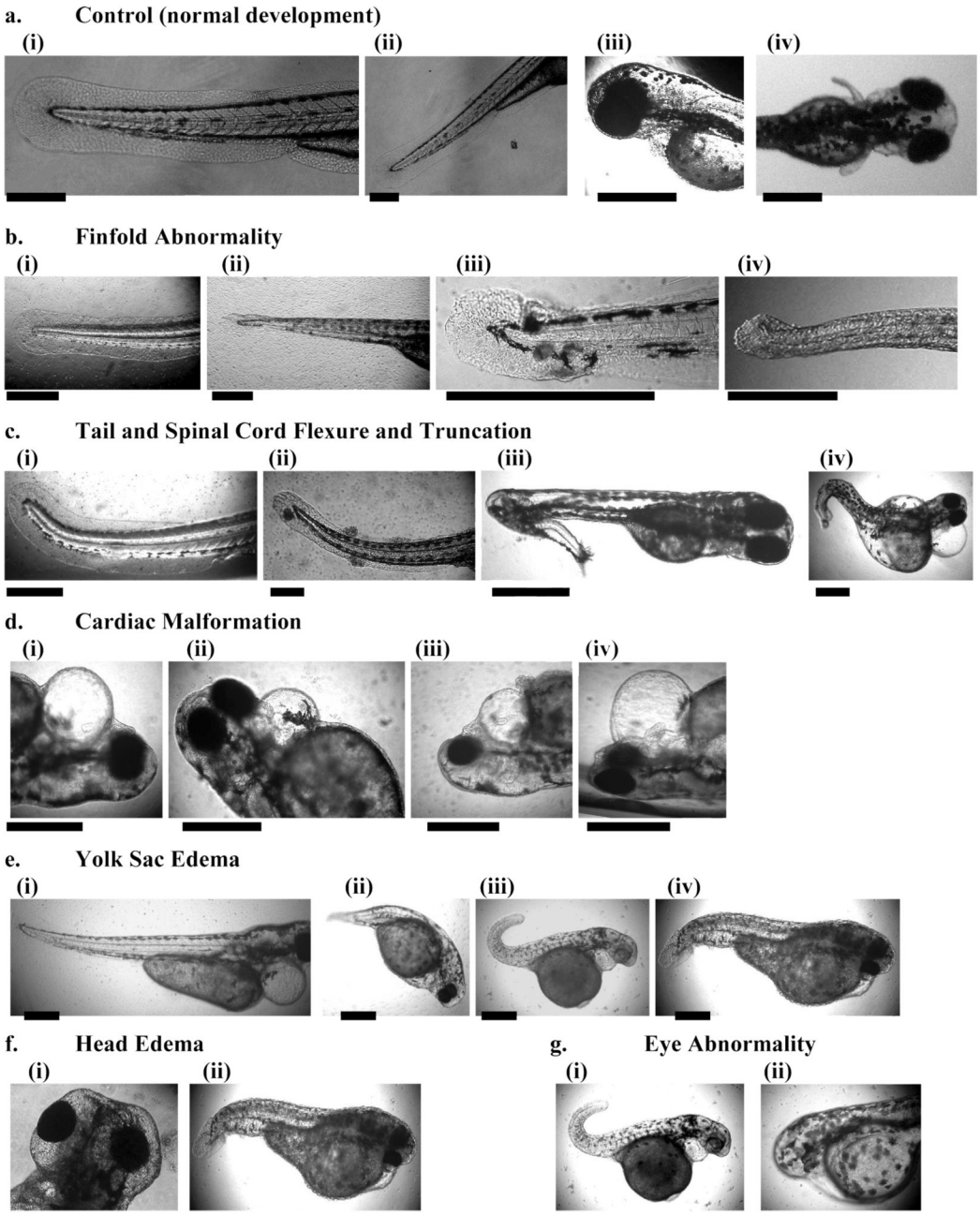

Figure 7. Biocompatibility and toxicity of nanoparticles show high dependence on nanoparticle concentration

(A) Histogram of distribution of normally developed (■) and dead (■) zebrafish, (a) versus concentration of Ag nanoparticles; (b) versus concentration of supernatants resulting from washing Ag nanoparticles (negative control); (c) histogram of distribution of deformed zebrafish (120 hpf) (■) versus concentration of Ag nanoparticles; (d) histogram of distribution of five representative types of deformities of the zebrafish versus concentration of Ag nanoparticles: finfold abnormality (■), tail and spinal cord flexure and truncation (■), cardiac malformation (■), yolk sac edema (■), head edema (■), and eye abnormality (■).

(B) Representative optical images of (a) normally developed and (b–g) deformed zebrafish: (a) the normal development of (i) finfold, (ii) tail/spinal cord, (iii) cardiac, (iii–iv) yolk sac, cardiac, head and eye; and (b–g) deformed zebrafish: (b) finfold abnormality; (c) tail and spinal cord flexure and truncation; (d) cardiac malformation; (e) yolk sac edema; (f) head edema: (i) head edema; (ii) head edema and eye abnormality; (g) eye abnormality: (i) eye abnormality; (ii) eyeless. Scale bar = 500 μm. More deformed zebrafish observed from these experiments are summarized in Table I of on-line SI.